



Article

Static and Dynamic Magnetic Properties of Fe₃O₄ Nanotubes

Francisco Olea de la Hoz¹, Eduardo Saavedra¹ , Alejandro Pereira² and Juan Escrig^{1,3,*} ¹ Department of Physics, University of Santiago de Chile (USACH), Santiago 9170124, Chile² Department of Sciences, Faculty of Liberal Arts, Adolfo Ibañez University (UAI), Santiago 7941169, Chile³ Center for the Development of Nanoscience and Nanotechnology (CEDENNA), Santiago 9170124, Chile

* Correspondence: juan.escrig@usach.cl; Tel.: +56-2-2718-3419

Abstract: In this paper, our objective was to investigate the static and dynamic magnetic properties of Fe₃O₄ nanotubes that are 1000 nm long, by varying the external radius and the thickness of the tube wall. We performed a detailed numerical analysis by simulating hysteresis curves with an external magnetic field applied parallel to the axis of the tubes (along the z-axis). Our findings indicate that nanotubes with an external radius of 30 nm exhibit non-monotonic behavior in their coercivity due to a change in the magnetization reversal mechanism, which was not observed in nanotubes with external radii of 80 nm. Additionally, we explored the dynamic susceptibility of these nanotubes and found that the position and number of resonance peaks can be controlled by manipulating the nanotube geometry. Overall, our study provides valuable insights into the behavior of Fe₃O₄ nanotubes, which can aid in the design and improvement in pseudo-one-dimensional technological devices.

Keywords: magnetic properties; Fe₃O₄; magnetic nanotubes; hysteresis curves; FMR

1. Introduction

When materials are reduced to the nanoscale, new properties emerge that differ from those exhibited by the same larger materials, as the characteristic dimensions of many physical phenomena are in the order of nanometers. These novel properties have enabled magnetic nanostructures to be utilized in various applications, including magnetic sensors, information storage systems, and spintronic-based devices, as well as medical applications such as hyperthermia or drug delivery. Going a step further, Niknam et al. [1] have recently proposed the use of nanomagnets for the quantum control of spin qubits, essential components of universal quantum computers. Proper control of the shape and size of these magnetic nanostructures can facilitate the design of innovative devices [2].

One of the most extensively studied magnetic nanostructures is magnetic nanotubes (MNTs) due to their high aspect ratio, similar to that of nanowires, but with two functionalizable surfaces [3]. Moreover, Yan et al. [4] have demonstrated that domain walls in a tubular geometry are more durable than those in flat strips, which can even suppress the Walker breakdown in these nanostructures. Bao et al. [5] proposed using ferromagnetic nanotubes as alternative skyrmion guides, which are a promising candidate for information carriers, while Yang et al. [6] investigated the stability of skyrmion formation in magnetic nanotubes. Additionally, Rojas-Nunez et al. [7] has shown that magnetic nanotubes provide a lightweight alternative for designing mechanical nanodevices with minimal loss of mechanical performance.

The field of magnetic nanotube synthesis has yielded a wide variety of materials that have been successfully utilized in the creation of these structures. Among the most commonly synthesized magnetic nanotubes are those made from materials such as iron (Fe) [8,9], Fe(OH)₃ [10], maghemite (γ-Fe₂O₃) [10–12], magnetite (Fe₃O₄) [10,12–18], ZnFe₂O₄ [19], CuFe₂O₄ [20], nickel (Ni) [8,21–23], NiFe₂O₄ [24], Ni₆₄Fe₃₆ [8], Ni₈₀Fe₂₀ (permalloy) [25], Co [8,23,26], Co₃O₄ [27], Co₉₀Pt₁₀ [8], Co₇₅Cr₁₃Pt₁₂ [8], and many others. In addition to these common materials, nanotubes with more complex geometries have also been



Citation: Olea de la Hoz, F.; Saavedra, E.; Pereira, A.; Escrig, J. Static and Dynamic Magnetic Properties of Fe₃O₄ Nanotubes. *Nanomaterials* **2023**, *13*, 1265. <https://doi.org/10.3390/nano13071265>

Academic Editor: Marius Dobromir

Received: 20 February 2023

Revised: 22 March 2023

Accepted: 23 March 2023

Published: 3 April 2023



Copyright: © 2023 by the authors. Licensee MDPI, Basel, Switzerland. This article is an open access article distributed under the terms and conditions of the Creative Commons Attribution (CC BY) license (<https://creativecommons.org/licenses/by/4.0/>).

synthesized, taking into consideration factors such as diameter modulations [28], multisegmented structures [29], and core–shell [30–33] systems. The synthesis of these advanced structures is a testament to the ingenuity and skill of researchers in this field, and it suggests that the possibilities for the creation of new and innovative magnetic nanotubes are practically limitless.

On the other hand, the static and dynamic magnetic properties of magnetic nanotubes, such as the magnetic equilibrium states [34–38], magnetization reversal mechanisms [16,17,21,23,37–43] and magnetostatic interaction [44–47], have also been investigated theoretically. González et al. [48] went further and calculated the spin wave spectra associated with the vortex domain wall confined within a nanotube, which encouraged the synthesis of Fe₃O₄ nanotubes with this type of domain wall [49]. Salazar-Cardona et al. [50] proposed a device based on coplanar waveguides that would selectively measure the exchange or dipole-induced spin wave nonreciprocities. Recently, some of us analyzed the dynamic susceptibility of curved permalloy nanotubes [51] and permalloy wire-tube nanostructures [52]. However, to the best of our knowledge, there are no studies that systematically investigate the static and dynamic properties of Fe₃O₄ nanotubes, despite the high aspect ratio being conducive to electron conduction and further increasing the conduction loss capability [53].

In this study, we investigate the static and dynamic magnetic response of long Fe₃O₄ nanotubes using micromagnetic simulations. Our objective is to examine how the magnetic properties vary with changes in the external radius and thickness of the tube wall. We focus particularly on the different magnetization reversal mechanisms and potential resonance modes that may appear.

2. Micromagnetic Simulations

The static and dynamic magnetic properties of a Fe₃O₄ nanotube (Figure 1) were studied using micromagnetic simulations performed using the mumax³ software [54], which solves the Landau–Lifshitz–Gilbert equation (LLG) [55]. The micromagnetic simulations were performed on a computer specifically configured to work with an RTX 3090 video card, which is ideal for running Mumax³ software in CUDA language. This RTX 3090 card has 10,752 CUDA cores, making it one of the best options for GPU-based micromagnetic studies.

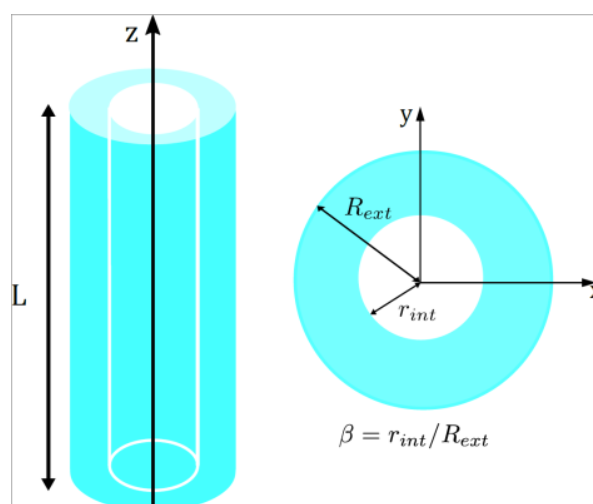


Figure 1. Schematic representation of an isolated magnetic nanotube. Representative geometric parameters are indicated.

For spherical nanoparticles, there is a critical diameter that allows discriminating between a superparamagnetic phase and a single-domain phase, which is approximately 30 nm for Fe₃O₄ nanoparticles [56]. However, in the case of pseudo-one-dimensional

nanostructures such as nanotubes, we almost always face a single-domain phase due to the large aspect ratio of this nanostructure. In this article, we consider a length of 1000 nm because Xiang et al. [57] have shown that the coercivity of a 20 nm diameter Fe nanowire does not vary for lengths greater than 200 nm. In fact, to ensure that this behavior is also valid for Fe₃O₄, we simulated 30 nm diameter nanowires with three different hole sizes, $\beta = 0.1, 0.5,$ and 0.9 , with lengths ranging between 1000 and 5000 nm (see Figure A1 of Appendix A). We considered two possible external radii, $R_{ext} = 30$ and 80 nm, and a variable internal radius, r_{int} , which allowed us to define the ratio $\beta = r_{int}/R_{ext}$ such that $\beta = 0$ represents a solid cylinder and $\beta \rightarrow 1$ corresponds to a very narrow tube (Figure 1). According to Escrig et al. [16], 80 nm diameter nanotubes are wide enough to reverse their magnetization through the nucleation and propagation of vortex domain walls, whereas thin 30 nm nanotubes can reverse their magnetization through transverse domain walls for small holes and vortex domain walls for large holes. Therefore, we have chosen well-differentiated diameters to see how this change in the reversal modes affects the static and dynamic magnetic properties of the nanotubes.

The magnetic parameters used for magnetite (Fe₃O₄) were the saturation magnetization $M_s = 4.8 \times 10^5$ A/m, the stiffness constant $A = 2.64 \times 10^{-11}$ J/m, and the cubic magnetocrystalline anisotropy $K_c = -1.25 \times 10^4$ J/m³ [58]. In the simulations, we used a cell size of $2 \times 2 \times 5$ nm³, which is small enough to accurately capture the geometry of the nanostructures. To simulate the magnetic configurations of minimum energy and the hysteresis loops (static magnetic properties), we used a large value of $\alpha = 0.5$, which is commonly used to reduce simulation time without significantly affecting the results of quasi-static simulations. The external magnetic field was applied parallel to the z -axis ($\theta = 0^\circ$) with a magnitude of $H = 1000$ mT to saturate the samples, and field steps of 2 mT were used to investigate the hysteresis curves.

On the other hand, to simulate the dynamic response of magnetization (FMR spectra), we used $\alpha = 0.015$ [59]. In addition, we applied a sinc wave excitation field [51]

$$h_{sinc} = h_0 \frac{\sin(2\pi f_c \tau)}{2\pi f_c \tau}$$

along the y -direction to perturb the magnetization of the system. The sinc function is a mathematical function used to describe the spectral response of a low-pass filter or the pulse response of a sampling system. In this equation, $h_0 = 5$ mT is the amplitude of the sinc function at its peak, the cut-off frequency is $f_c = 45$ GHz, and $\tau = t - t_0$ was the simulation time (t), with an offset t_0 . The data in the time domain were recorded for 20 ns with a step time of 10 ps, allowing for a better spectral resolution of 0.05 GHz. For FMR analysis, we derived the imaginary part of the dynamical susceptibility via a fast-Fourier transform (FFT) procedure. Specifically, the frequency-dependent magnetic susceptibility of a material, $\chi(\omega)$, is defined as the ratio of the Fourier component, $m_y(\omega)$, of the y -component of the spatially averaged magnetization $m(t)$ and the Fourier component, $h(\omega)$, of the applied exciting field [60],

$$\chi(\omega) = m_y(\omega)/h(\omega).$$

We further obtained the spatial FMR mode profiles from the post-processing of the position-dependent magnetization data. The magnetic susceptibility is a fundamental property of magnetic materials that determines how they respond to magnetic fields. It is used to characterize the magnetic properties of materials in a variety of applications, including magnetic storage, magnetic resonance imaging, and magnetic sensors. The equation is often used in the analysis of magnetic materials and in the design of magnetic devices.

3. Results and Discussion

In this section, we present and analyze the results of our micromagnetic simulations for the static and dynamic properties of Fe₃O₄ nanotubes. For the static behavior, we focus on the coercivity, remanence, and magnetization reversal modes. For the dynamic behavior,

we analyze the dynamic susceptibility and the resonant frequencies of the peaks for the different geometric parameters considered.

3.1. Static Magnetic Properties

In the first stage, we obtained the hysteresis curves of Fe_3O_4 nanotubes with a length of 1000 nm for two different external radii, $R_{\text{ext}} = 30$ nm (Figure 2a) and $R_{\text{ext}} = 80$ nm (Figure 2b), considering different tube walls by varying the $\beta = r_{\text{int}}/R_{\text{ext}}$ value. The hysteresis curves shown in Figure 2a,b differ due to the use of different diameters (see Figure 3 of Ref. [57]). Figure 2a shows that nanotubes with an external radius of 30 nm present square hysteresis curves, with significant coercivities (H_c) and normalized remanences (M_r/M_s) very close to 1.0. The appearance of a small hole ($\beta = 0.2$) produces a slight increase in coercivity when compared to the coercivity produced by a nanowire ($\beta = 0.0$). However, for larger holes ($\beta \geq 0.4$), the coercivity begins to decrease drastically. To explain this non-monotonic behavior, in Appendix A we plotted the magnetization reversal process of these nanotubes as a function of time (see Figure A2). From Figure A2a, we can see that a nanowire ($\beta = 0.0$) reverses its magnetization via nucleation and propagation of two transverse domain walls in the caps that propagate towards the center of the nanowire. Figure A2b shows that in the case of a nanotube with a small hole ($\beta = 0.2$), the system keeps reversing its magnetization via transverse domain walls. However, due to the new inner surface, the magnetic moments are not perfectly aligned, resulting in a slight increase in coercivity. Figure A2c shows that a nanotube with a larger hole ($\beta = 0.4$) nucleates transverse domain walls at the caps, which, as they propagate towards the center of the nanotube, become vortex walls, speeding up the magnetization reversal process and allowing a decrease in the coercivity of the system. It is also interesting to note that a step appears in the hysteresis curve for larger holes, whose size increases as the size of the hole increases. A similar behavior where nanotubes reverse their magnetization through different reversal mechanisms as a function of the tube wall width was previously observed [16,17].

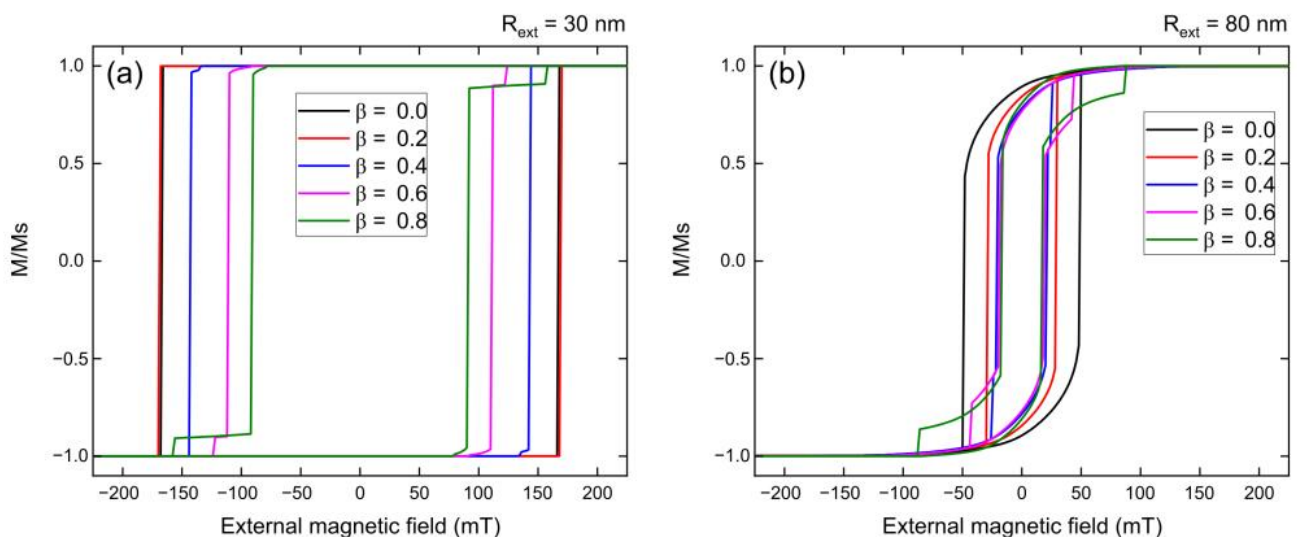


Figure 2. Hysteresis curves for 1000 nm long Fe_3O_4 nanotubes with external radius: (a) $R_{\text{ext}} = 30$ nm and (b) $R_{\text{ext}} = 80$ nm, for different β values, when the external magnetic field is applied along the z-axis.

In contrast, Figure 2b shows that Fe_3O_4 nanotubes with an external radius of 80 nm exhibit more rounded hysteresis curves, with lower coercivities (H_c) and normalized remanences (M_r/M_s) compared to those observed for nanotubes with an external radius of 30 nm. Additionally, it is observed that these larger nanotubes also display a step in their hysteresis curve, for practically all values of β . To explain these behaviors, we have graphed the magnetization reversal process of these nanotubes as a function of time in Appendix A.

From Figure A3a–c, we observe that both nanowire ($\beta = 0.0$) and nanotubes ($\beta = 0.1$ and 0.2) reverse their magnetization by nucleating and propagating two vortex domain walls at the caps that propagate towards the center of the nanostructure. This implies that for this outer radius, there is a unique magnetization reversal mechanism, which is why the coercivity decreases monotonically as we increase the value of β . Furthermore, Figure A3b,c indicate that the steps that appear in the hysteresis curves are due to the collision between the two vortices with different chiralities in the center of the nanotube, which requires a larger field for complete annihilation.

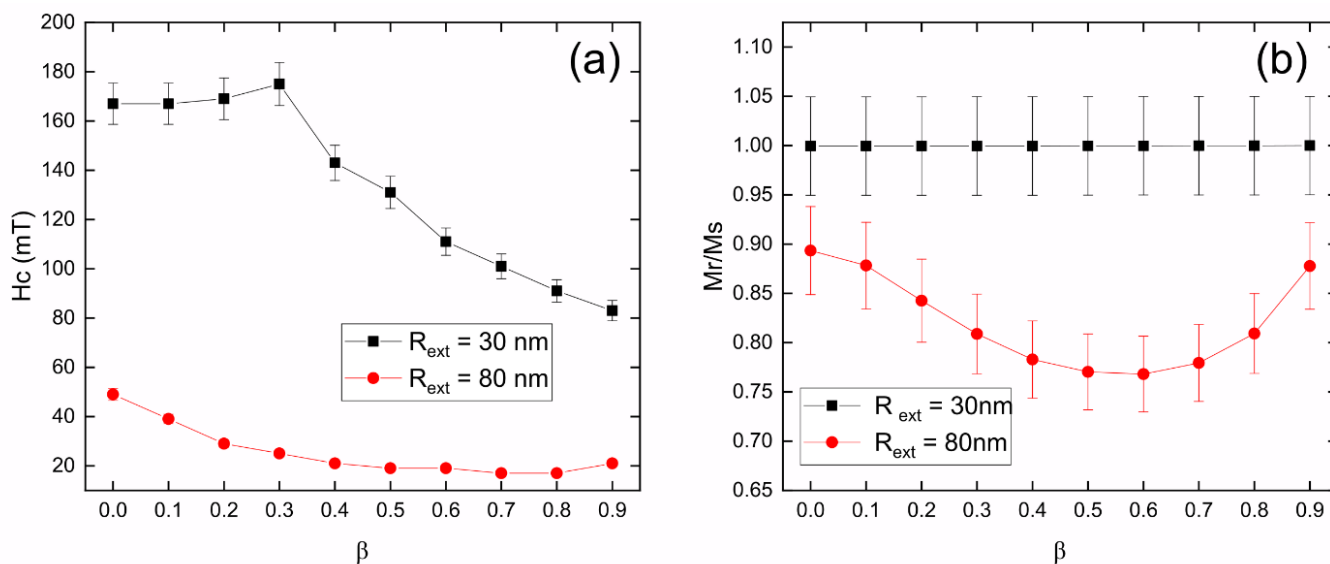


Figure 3. (a) Coercivity and (b) normalized remanence for 1000 nm long Fe_3O_4 nanotubes with external radius 30 nm (black squares) and 80 nm (red circles), as a function of β , when the external magnetic field is applied along the z-axis. We considered an error of 5%.

Figure 3 displays the coercivity and normalized remanence for 1000 nm long Fe_3O_4 nanotubes with an external radius of 30 nm and 80 nm, as a function of β , when the external magnetic field is applied along the z-axis. From Figure 3a, it is evident that the coercivity of nanotubes with an external radius of 30 nm is consistently higher than the coercivity of nanotubes with an external radius of 80 nm, irrespectively of the value of β . Additionally, we observe that the coercivity of nanotubes with an external radius of 30 nm follows a non-monotonic behavior, reaching a maximum value close to 180 mT for $\beta = 0.3$, and beyond which it starts decreasing until reaching approximately 80 mT for $\beta = 0.9$. This non-monotonic behavior is due to the fact that nanotubes with $\beta < 0.4$ reverse their magnetization through transverse domain walls, while nanotubes with $\beta \geq 0.4$ reverse their magnetization through vortex domain walls. From Figure 3b, we see that these nanotubes with an external radius of 30 nm exhibit a normalized remanence equal to 1.0 for all β values, which explains the square behavior of the hysteresis curves shown in Figure 2a.

Figure 3a indicates that the coercivity of 80 nm outer radius nanotubes decreases as a function of β , from approximately 50 mT for $\beta = 0.0$ to almost 20 mT for $\beta = 0.8$. This can be explained by the fact that these nanotubes reverse their magnetization through the nucleation and propagation of vortex domain walls. On the other hand, Figure 3b shows that the normalized remanence exhibits a non-monotonic behavior as a function of β , with values close to 0.9 for $\beta = 0.0$ and 0.9 , and a value that reduces to a valley close to 0.75 for $\beta = 0.6$. This explains the more rounded behavior exhibited by the hysteresis curves shown in Figure 2b.

3.2. Dynamic Magnetic Properties

To investigate the magnetization dynamics of 1000 nm long Fe_3O_4 nanotubes, we carried out ferromagnetic resonance (FMR) studies on the remanent state of each geometry (see Figure A4 in Appendix A). Subsequently, we investigated the dynamic susceptibility of nanotubes with an external radius of 30 and 80 nm by applying a sinc wave excitation in the y -direction. Figure 4a shows the resonant modes for the nanowire ($\beta = 0.0$) with an external radius of 30 nm. We can observe two well-defined modes, one of low frequency mode edge (mode E), associated with the caps of the nanowire, and another of high frequency mode bulk (mode B), of greater height, as it excites a larger number of magnetic moments associated with the central area of the nanowire. The latter presents a small bump that we have defined as the mode ring (mode R), which is associated with a disturbance close to the edges of the wire. On the other hand, Figure 4b shows the resonant modes for the nanowire ($\beta = 0.0$) with an external radius of 80 nm. In this case, we can see that the number of modes increases, where seven modes are clearly identified, and among which we can again highlight the low frequency mode, mode E, and the high frequency mode, mode B. In this last mode, the bump we called mode R does not appear, but we can observe a similar behavior in mode 6. The increase in the number of modes that occurs when we go from a thin nanotube to a thick one is expected. Lupo et al. [61] investigated the radial and azimuthal resonance modes of spin waves in $\text{Ni}_{80}\text{Fe}_{20}$ (permalloy) nanodisks in the absence of an external magnetic field, finding that the number of absorption modes increased as the disk diameter increased. A similar conclusion was reached by Dobrovolskiy et al. [62], who investigated Co-Fe nanodisks. In fact, we have shown in Figure A5 of Appendix A that the number of resonance modes increases as the diameter of the nanotubes increases. It is evident from the FFT power distributions that each mode can be characterized by the number of nodes (N) present along the longitudinal axis of the nanotube [63].

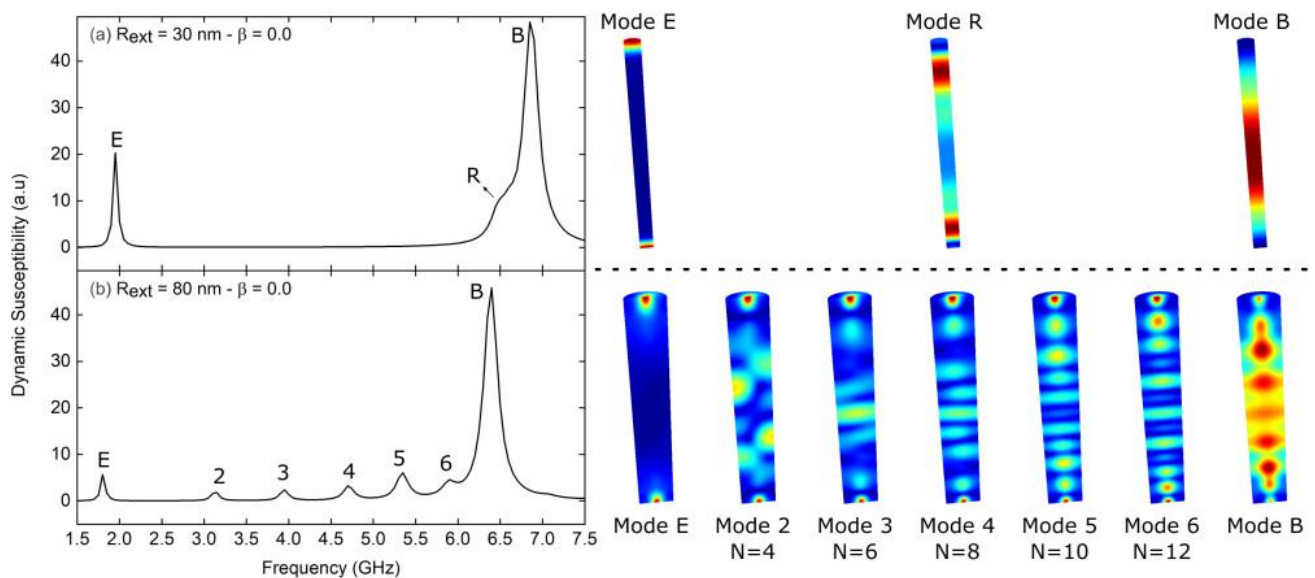


Figure 4. Dynamic susceptibility spectra for 1000 nm long Fe_3O_4 nanotubes with external radius (a) $R_{\text{ext}} = 30 \text{ nm}$ and (b) $R_{\text{ext}} = 80 \text{ nm}$, for $\beta = 0.0$, while the system is excited with a sinc wave field in the y -direction. On the right are the spatial profiles of the resonant modes shown to the left. The color scale corresponds to the amplitude of the magnetic moment fluctuations, with red depicting the largest amplitude and blue denoting zero amplitude.

In Figure 5, we can observe how these modes change with respect to β . In Figure 5a, it is shown that mode R, which corresponds to a bump of mode B, almost disappears for $\beta \geq 0.4$. This implies that nanotubes with an external radius of 30 nm with large holes only exhibit two resonance modes, namely mode E and mode B. As the value of β increases, both modes move closer towards intermediate frequencies. In Figure 5b, it is noticeable

that the seven modes that appear for $\beta = 0.0$ change remarkably, with only modes E, 2, 3, and 4 surviving for $\beta = 0.8$. In fact, the mode that stands out the most for $\beta = 0.0$, mode B, only survives for small β values.

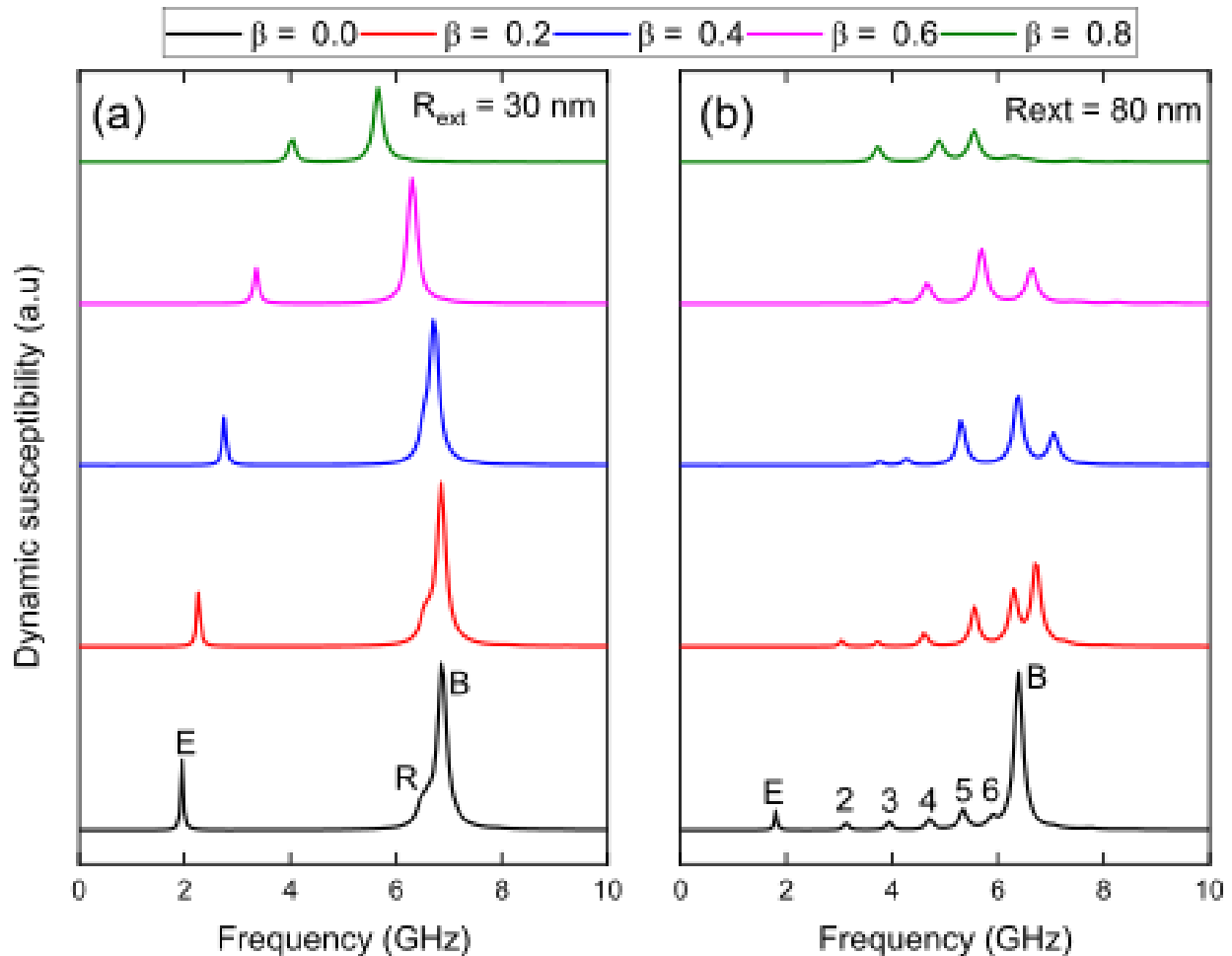


Figure 5. Evolution of dynamic susceptibility spectra for 1000 nm long Fe_3O_4 nanotubes with external radius (a) $R_{\text{ext}} = 30$ nm and (b) $R_{\text{ext}} = 80$ nm, as a function of β values. The system is excited with a sinc wave field in the y -direction.

Figure 6 shows the evolution of resonance modes for Fe_3O_4 nanotubes of length 1000 nm and external radii of 30 and 80 nm, as a function of the parameter β . It can be observed from this figure that mode E increases monotonically from approximately 2.0 GHz for $\beta = 0.0$ to 4.5 GHz for $\beta = 0.9$ when the external radius is 30 nm. However, when the nanotube has an external radius of 80 nm, the same resonance mode follows a non-monotonic behavior, reaching a maximum value of approximately 4.0 GHz for $\beta = 0.6$. Mode B monotonically decreases from approximately 7.0 GHz for $\beta = 0.0$ to 5.0 GHz for $\beta = 0.9$ when the external radius is 30 nm, while this mode experiences a sustained increase when the external radius is 80 nm, disappearing for $\beta \geq 0.6$. Figure 6a also shows that mode R remains stable around 6.5 GHz for $\beta \leq 0.3$, while modes 2, 3, and 4 observed in Figure 6b follow a similar non-monotonic behavior as mode E, and modes 5 and 6, grow monotonically with β but do not exist for the entire investigated range, similar to what occurs with mode B.

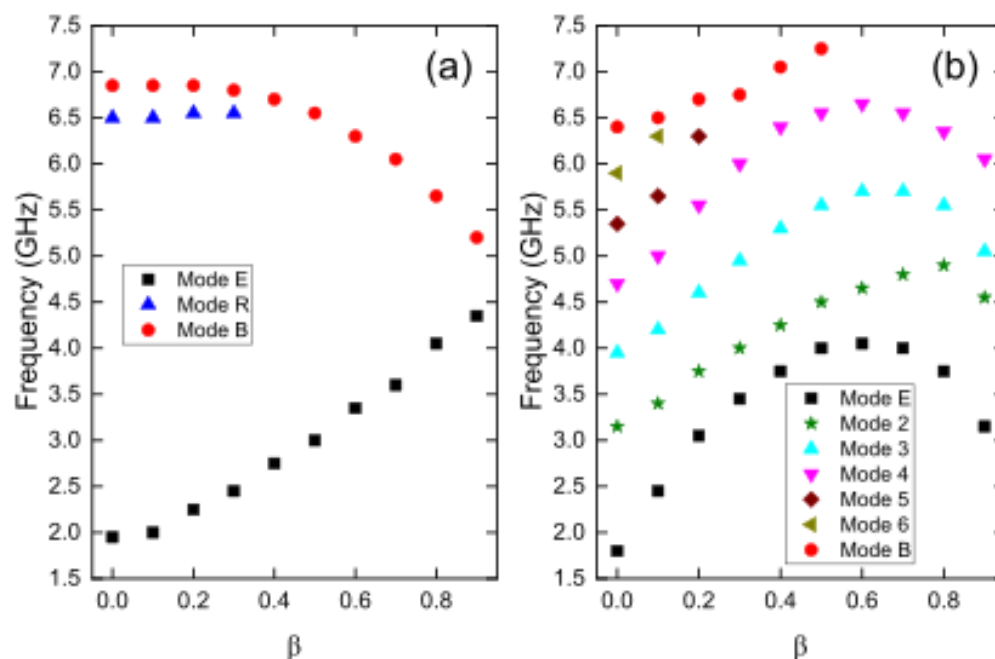


Figure 6. Evolution of resonance modes for 1000 nm long Fe_3O_4 nanotubes with external radius (a) $R_{ext} = 30$ nm and (b) $R_{ext} = 80$ nm, as a function of the parameter β .

4. Conclusions

In summary, this study used micromagnetic simulations to investigate the static and dynamic magnetic properties of Fe_3O_4 nanotubes with varying external radii and tube wall thicknesses. Our findings revealed that the coercivity and remanence of the nanotubes are non-zero when a magnetic field is applied parallel to the tube axis. The coercivity of the 30 nm nanotubes exhibited a non-monotonic behavior, while the coercivity of the 80 nm nanotubes decreased monotonically with increasing β . We also found that the geometry of the nanotubes can be used to control the number of resonance modes and their frequencies, making them a potential candidate for use in microwave devices.

Overall, this study contributes to the understanding of the magnetic properties of Fe_3O_4 nanotubes and demonstrates the potential for their use in practical applications.

Author Contributions: Conceptualization, J.E.; data curation, F.O.d.I.H., A.P. and E.S.; formal analysis, F.O.d.I.H., A.P. and E.S.; funding acquisition, J.E.; investigation, F.O.d.I.H., A.P. and E.S.; methodology, J.E. and E.S.; project administration, J.E.; resources, J.E. and A.P.; software, E.S.; supervision, J.E.; validation, F.O.d.I.H., A.P. and E.S.; visualization, J.E. and E.S.; writing—original draft preparation, E.S. and J.E.; writing—review and editing, J.E. and E.S. All authors have read and agreed to the published version of the manuscript.

Funding: This research was funded by Fondecyt (grant number 1200302), Dicyt-Usach (grant number 042331SD and APC payment) and Financiamiento Basal para Centros Científicos y Tecnológicos (grant number AFB220001).

Institutional Review Board Statement: Not applicable.

Informed Consent Statement: Not applicable.

Data Availability Statement: Data will be made available upon request.

Conflicts of Interest: The authors declare that they have no known competing financial interests or personal relationships that could have appeared to influence the work reported in this paper.

Appendix A

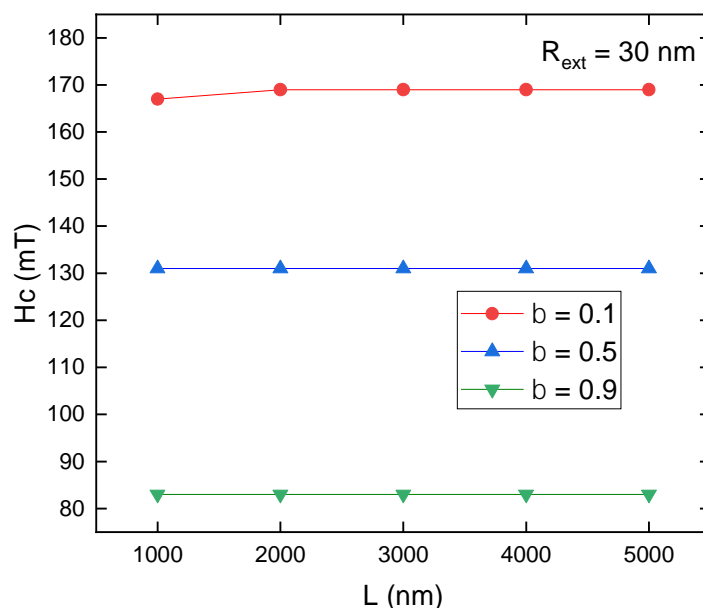


Figure A1. Coercivity for long Fe₃O₄ nanotubes with an external radius of 30 nm and three different hole sizes, $\beta = 0.1, 0.5,$ and $0.9,$ with lengths ranging between 1000 and 5000 nm, when the external magnetic field is applied along the z-axis.

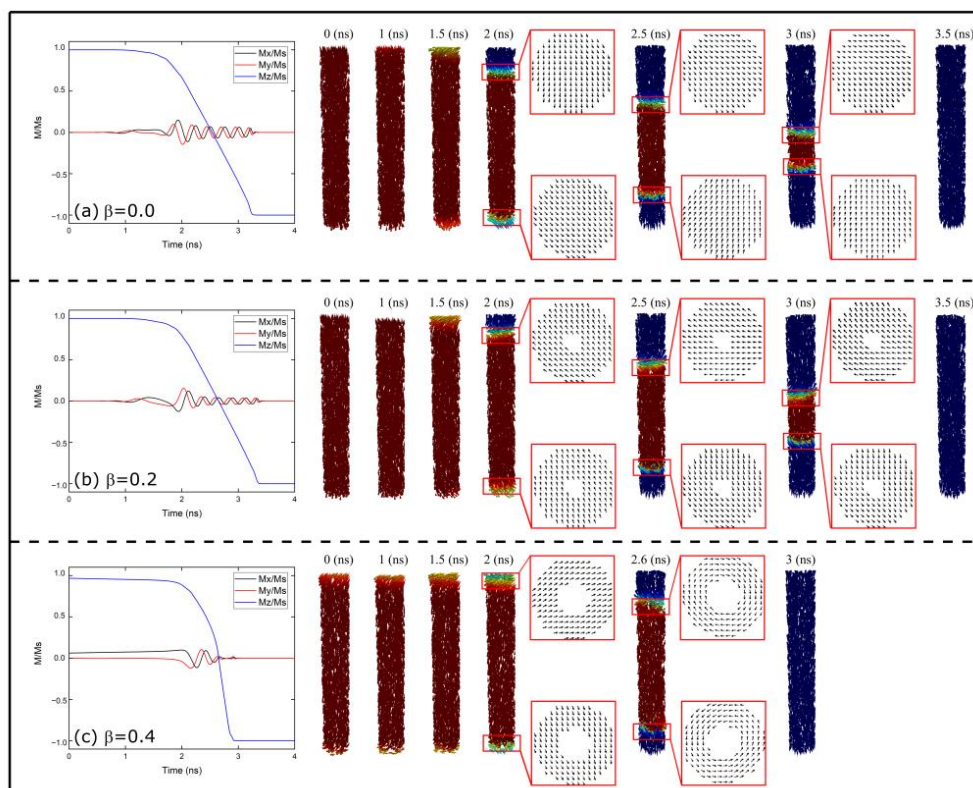


Figure A2. Magnetization reversal of a 1000 nm long Fe₃O₄ nanotube with an external radius of 30 nm, for $\beta = 0.0$ (a), 0.2 (b), and 0.4 (c). The graphs on the left depict the components of magnetization as a function of time, while the snapshots of magnetization at specific times are presented on the right of each graph.

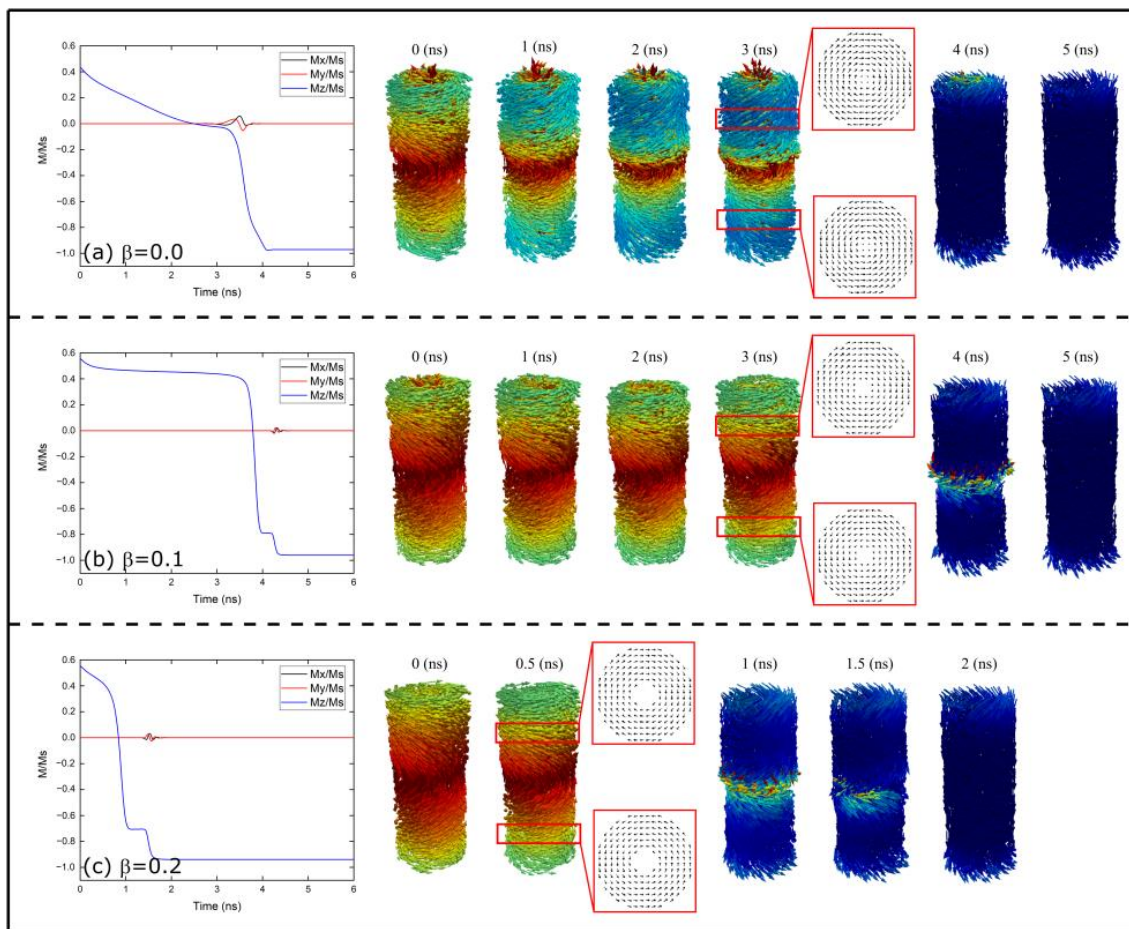


Figure A3. Magnetization reversal of a 1000 nm long Fe_3O_4 nanotube with an external radius of 80 nm, for $\beta = 0.0$ (a), 0.1 (b), and 0.2 (c). The graphs on the left depict the components of magnetization as a function of time, while the snapshots of magnetization at specific times are presented on the right of each graph.

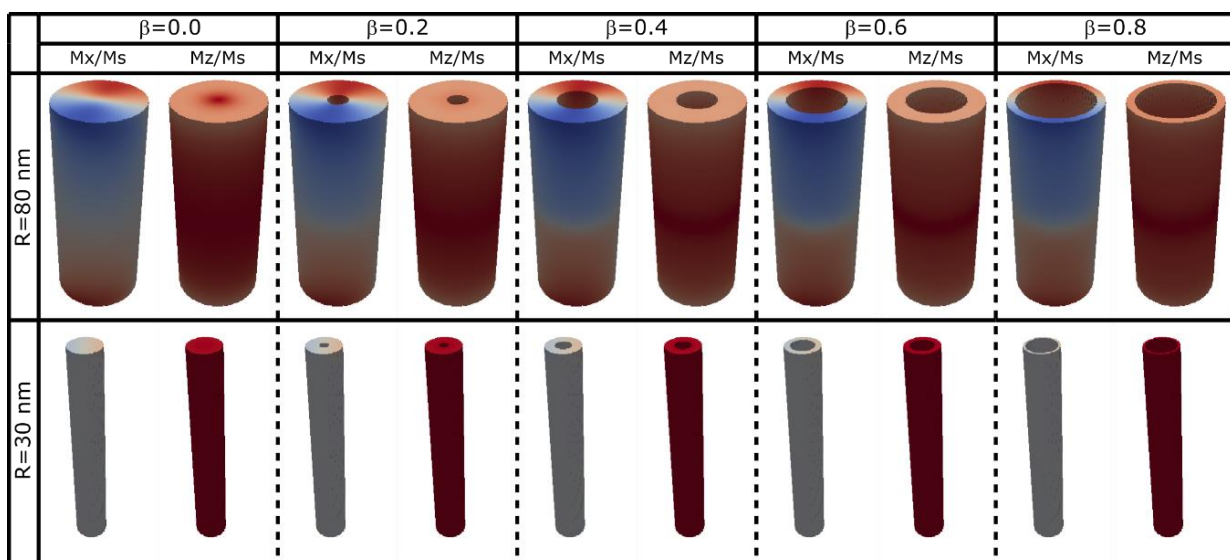


Figure A4. Components of the magnetization (Mx/Ms and Mz/Ms) for each of the geometries that were excited to investigate the FMR spectrum of the 1000 nm long Fe_3O_4 nanotubes.

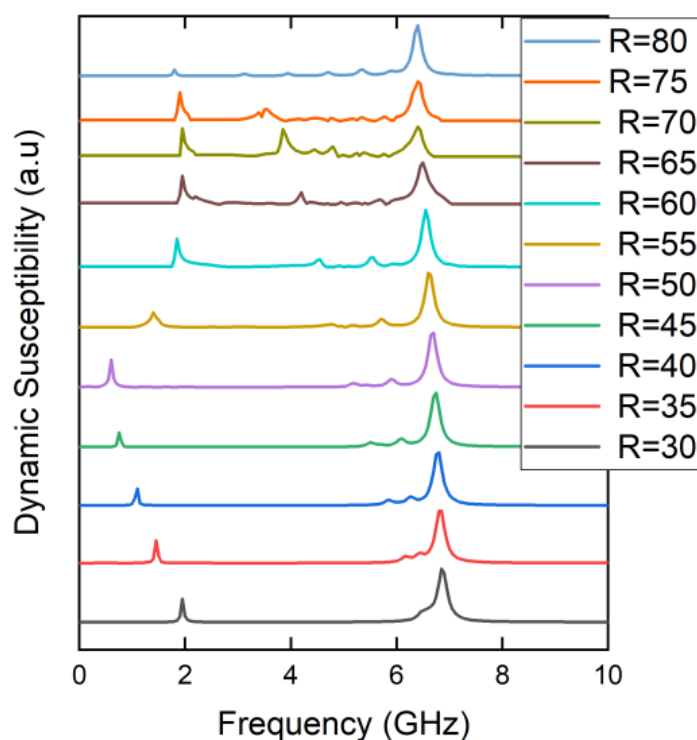


Figure A5. Dynamic susceptibility spectra for 1000 nm long Fe_3O_4 nanotubes with different radii ranging between 30 and 80 nm, for different β values, while the system is excited with a sinc wave field in the y -direction.

References

- Nikman, M.; Chowdhury, M.F.F.; Rajib, M.M.; Misba, W.A.; Schwartz, R.N.; Wang, K.L.; Atulasimha, J.; Bouchard, L.S. Quantum control of spin qubits using nanomagnets. *Commun. Phys.* **2022**, *5*, 284.
- Nguyen, M.D.; Tran, H.V.; Xu, S.; Lee, T.R. Fe_3O_4 nanoparticles: Structures, synthesis, magnetic properties, Surface functionalization, and emerging applications. *Appl. Sci.* **2021**, *11*, 11301. [[CrossRef](#)] [[PubMed](#)]
- Ye, Y.; Geng, B. Magnetic nanotubes: Synthesis, properties, and applications. *Crit. Rev. Solid State Mater. Sci.* **2012**, *37*, 75. [[CrossRef](#)]
- Yan, M.; Andreas, C.; Kakay, A.; García-Sánchez, F.; Hertel, R. Fast domain wall dynamics in magnetic nanotubes: Suppression of Walker breakdown and Cherenkov-like spin wave emission. *Appl. Phys. Lett.* **2011**, *99*, 122505. [[CrossRef](#)]
- Bao, B.; Yang, M.; Yan, M. Asymmetric motion of magnetic skyrmions in ferromagnetic nanotubes induced by a magnetic field. *Symmetry* **2022**, *14*, 1195. [[CrossRef](#)]
- Yang, J.; Kim, J.; Abert, C.; Suess, D.; Kim, S.K. Stability of skyrmion formation and its abnormal dynamic modes in magnetic nanotubes. *Phys. Rev. B* **2020**, *102*, 094439. [[CrossRef](#)]
- Rojas-Nunez, J.; Valencia, F.; Gonzalez, R.I.; Bringa, E.M.; Allende, S.; Palma, J.L.; Pereira, A.; Escrig, J.; Baltazar, S.E. Mechanical performance of lightweight polycrystalline Ni nanotubes. *Comput. Mater. Sci.* **2019**, *168*, 81. [[CrossRef](#)]
- Han, X.F.; Shamaila, S.; Sharif, R.; Chen, J.Y.; Liu, H.R.; Liu, D.P. Structural and magnetic properties of various ferromagnetic nanotubes. *Adv. Mater.* **2009**, *21*, 4619. [[CrossRef](#)]
- Xu, Y.; Xue, D.S.; Fu, J.L.; Gao, D.Q.; Gao, B. Synthesis, characterization and magnetic properties of Fe nanotubes. *J. Phys. D Appl. Phys.* **2008**, *41*, 215010. [[CrossRef](#)]
- Wang, Q.; Geng, B.; Wang, S.; Ye, Y.; Tao, B. Modified kirckendall effect for fabrication of magnetic nanotubes. *Chem. Commun.* **2010**, *46*, 1899. [[CrossRef](#)]
- Wang, J.; Ma, Y.; Watanabe, K. Magnetic-field-induced synthesis of magnetic $\gamma\text{-Fe}_2\text{O}_3$ nanotubes. *Chem. Mater.* **2008**, *20*, 20. [[CrossRef](#)]
- Lv, B.; Xu, Y.; Wu, D.; Sun, Y. Preparation and properties of magnetic iron oxide nanotubes. *Particuology* **2008**, *6*, 334. [[CrossRef](#)]
- Sui, Y.C.; Skomski, R.; Sorge, K.D.; Sellmyer, D.J. Magnetic nanotubes produced by hydrogen reduction. *J. Appl. Phys.* **2004**, *95*, 7151. [[CrossRef](#)]
- Son, S.J.; Reichel, J.; He, B.; Schuchman, M.; Lee, S.B. Magnetic nanotubes for magnetic-field-assisted bioseparation, biointeraction, and drug delivery. *J. Am. Chem. Soc.* **2005**, *127*, 7316. [[CrossRef](#)]
- Wang, T.; Wang, Y.; Li, F.; Xu, C.; Zhou, D. Morphology and magnetic behaviour of an Fe_3O_4 nanotube array. *J. Phys. Condens. Matter* **2006**, *18*, 10545. [[CrossRef](#)]

16. Escrig, J.; Bachmann, J.; Jing, J.; Daub, M.; Altbir, D.; Nielsch, K. Crossover between two different magnetization reversal modes in arrays of iron oxide nanotubes. *Phys. Rev. B* **2008**, *77*, 214421. [[CrossRef](#)]
17. Bachmann, J.; Escrig, J.; Pitzschel, K.; Montero Moreno, J.M.; Jing, J.; Gorlitz, D.; Nielsch, K. Size effects in ordered arrays of magnetic nanotubes. *J. Appl. Phys.* **2009**, *105*, 07B521. [[CrossRef](#)]
18. Wang, X.; Pan, F.; Xiang, Z.; Jia, W.; Lu, W. Magnetic Fe₃O₄@PVP nanotubes with high heating efficiency for MRI-guided magnetic hyperthermia applications. *Mater. Lett.* **2020**, *262*, 127187. [[CrossRef](#)]
19. Xu, Y.; Liang, Y.; Jiang, L.; Wu, H.; Zhao, H.; Xue, D. Preparation and magnetic properties of ZnFe₂O₄ nanotubes. *J. Nanomater.* **2011**, *2011*, 525967. [[CrossRef](#)]
20. Gao, H.; Gao, D.; Zhang, J.; Yang, G.; Zhang, J.; Shi, Z.; Xue, D. Synthesis and magnetic properties of CuFe₂O₄ nanotube arrays. *J. Wuhan Univ. Technol. Mater. Sci. Ed.* **2012**, *27*, 550. [[CrossRef](#)]
21. Escrig, J.; Daub, M.; Landeros, P.; Nielsch, K.; Altbir, D. Angular dependence of coercivity in magnetic nanotubes. *Nanotechnology* **2007**, *18*, 445706. [[CrossRef](#)]
22. Tao, F.F.; Xu, Z. Effective synthesis of magnetic metal nickel nanotubes. *Acta Phys. Chim. Sin.* **2009**, *25*, 977.
23. Proenca, M.P.; Sousa, C.T.; Ventura, J.; Araujo, J.P.; Escrig, J.; Vázquez, M. Crossover between magnetic reversal modes in ordered Ni and Co nanotube arrays. *Spin* **2012**, *2*, 1250014. [[CrossRef](#)]
24. Li, F.; Song, L.; Zhou, D.; Wang, T.; Wang, Y.; Wang, H. Fabrication and magnetic properties of NiFe₂O₄ nanocrystalline nanotubes. *J. Mater. Sci.* **2007**, *42*, 7214. [[CrossRef](#)]
25. Giordano, M.C.; Hamdi, M.; Mucchietto, A.; Grundler, D. Confined spin waves in magnetochiral nanotubes with axial and circumferential magnetization. *Phys. Rev. Mater.* **2023**, *7*, 024405. [[CrossRef](#)]
26. Sharif, R.; Shamaila, S.; Ma, M.; Yao, L.D.; Yu, R.C.; Han, X.F.; Khaleeq-ur-Rahman, M. Magnetic switching of ferromagnetic nanotubes. *Appl. Phys. Lett.* **2008**, *92*, 032505. [[CrossRef](#)]
27. Shen, X.P.; Miao, H.J.; Zhao, H.; Xu, Z. Synthesis, characterization and magnetic properties of Co₃O₄ nanotubes. *Appl. Phys. A* **2008**, *91*, 47. [[CrossRef](#)]
28. Pitzschel, K.; Montero Moreno, J.M.; Escrig, J.; Albrecht, O.; Nielsch, K.; Bachmann, J. Controlled introduction of diameter modulations in arrayed magnetic iron oxide nanotubes. *ACS Nano* **2009**, *3*, 3463. [[CrossRef](#)] [[PubMed](#)]
29. Leighton, B.; Suarez, O.J.; Landeros, P.; Escrig, J. Magnetic phase diagrams of barcode-type nanostructures. *Nanotechnology* **2009**, *20*, 385703. [[CrossRef](#)]
30. Zhu, C.L.; Zhang, M.L.; Qiao, Y.J.; Zhang, F.; Chen, Y.J. Fe₃O₄/TiO₂ core/shell nanotubes: Synthesis and magnetic and electromagnetic wave absorption characteristics. *J. Phys. Chem. C* **2010**, *114*, 16229. [[CrossRef](#)]
31. Pitzschel, K.; Bachmann, J.; Montero Moreno, J.M.; Escrig, J.; Gorlitz, D.; Nielsch, K. Reversal modes and magnetostatic interactions in Fe₃O₄/ZrO₂/Fe₃O₄ multilayer nanotubes. *Nanotechnology* **2012**, *23*, 495718. [[CrossRef](#)]
32. Shumskaya, A.; Korolkov, I.; Rogachev, A.; Ignatovich, Z.; Kozlovskiy, A.; Zdorovets, M.; Anisovich, M.; Bashouti, M.; Shalabny, A.; Busool, R.; et al. Synthesis of Ni@Au core-shell magnetic nanotubes for bioapplication and SERS detection. *Colloids Surf. A Physicochem. Eng. Asp.* **2021**, *626*, 127077. [[CrossRef](#)]
33. Pereira, A.; Escrig, J.; Palma, J.L.; López de Dicastillo, C.; Patiño, C.; Galotto, M.J. Magnetic nanotubes obtained from atomic layer deposition coated electrospun nanofibers. *J. Vac. Sci. Technol. B* **2018**, *36*, 061803. [[CrossRef](#)]
34. Chen, A.P.; Usov, N.A.; Blanco, J.M.; González, J. Equilibrium magnetization states in magnetic nanotubes and their evolution in external magnetic field. *J. Magn. Magn. Mater.* **2007**, *316*, e317–e319. [[CrossRef](#)]
35. Lee, J.; Suess, D.; Schrefl, T.; Oh, K.H.; Fidler, J. Magnetic characteristics of ferromagnetic nanotube. *J. Magn. Magn. Mater.* **2007**, *310*, 2445. [[CrossRef](#)]
36. Escrig, J.; Landeros, P.; Altbir, D.; Vogel, E.E.; Vargas, P. Phase diagrams of magnetic nanotubes. *J. Magn. Magn. Mater.* **2007**, *308*, 233. [[CrossRef](#)]
37. Chen, A.P.; Guslienko, K.Y.; Gonzalez, J. Magnetization configurations and reversal of thin magnetic nanotubes with uniaxial anisotropy. *J. Appl. Phys.* **2010**, *108*, 083920. [[CrossRef](#)]
38. Chen, A.P.; Gonzalez, J.M.; Guslienko, K.Y. Magnetization configurations and reversal of magnetic nanotubes with opposite chiralities of the end domains. *J. Appl. Phys.* **2011**, *109*, 073923. [[CrossRef](#)]
39. Landeros, P.; Allende, S.; Escrig, J.; Salcedo, E.; Altbir, D.; Vogel, E.E. Reversal modes in magnetic nanotubes. *Appl. Phys. Lett.* **2007**, *90*, 102501. [[CrossRef](#)]
40. Landeros, P.; Núñez, A. Domain wall motion on magnetic nanotubes. *J. Appl. Phys.* **2010**, *108*, 033917. [[CrossRef](#)]
41. Albrecht, O.; Zierold, R.; Allende, S.; Escrig, J.; Patzig, C.; Rauschenbach, B.; Nielsch, K.; Gorlitz, D. Experimental evidence for an angular dependent transition of magnetization reversal modes in magnetic nanotubes. *J. Appl. Phys.* **2011**, *109*, 093910. [[CrossRef](#)]
42. Arciniegas Jaimes, D.M.; Raviolo, S.; Carballo, J.M.; Bajales, N.; Escrig, J. Wave reversion mode stability as a function of diameter and wall thickness for permalloy and nickel nanotubes. *J. Magn. Magn. Mater.* **2021**, *523*, 167578. [[CrossRef](#)]
43. Raviolo, S.; Arciniegas Jaimes, D.M.; Bajales, N.; Escrig, J. Wave reversal mode: A new magnetization reversal mechanism in magnetic nanotubes. *J. Magn. Magn. Mater.* **2020**, *497*, 165944. [[CrossRef](#)]
44. Escrig, J.; Allende, S.; Altbir, D.; Bahiana, M. Magnetostatic interactions between magnetic nanotubes. *Appl. Phys. Lett.* **2008**, *93*, 023101. [[CrossRef](#)]
45. Suarez, O.J.; Vargas, P.; Vogel, E.E. Energy and force between two magnetic nanotubes. *J. Magn. Magn. Mater.* **2009**, *321*, 3658. [[CrossRef](#)]

46. Landeros, P.; Guzmán, P.R.; Soto-Garrido, R.; Escrig, J. Magnetostatic fields in tubular nanostructures. *J. Phys. D Appl. Phys.* **2009**, *42*, 225002. [[CrossRef](#)]
47. Morales-Concha, C.; Ossandón, M.; Pereira, A.; Altbir, D.; Escrig, J. General approach to the magnetostatic force and interaction between cylindrically shaped nanoparticles. *J. Appl. Phys.* **2012**, *111*, 07D131. [[CrossRef](#)]
48. González, A.L.; Landeros, P.; Núñez, A.S. Spin wave spectrum of magnetic nanotubes. *J. Magn. Magn. Mater.* **2010**, *322*, 530. [[CrossRef](#)]
49. Zhang, R.; Wang, L.; Xu, C.; Liang, C.; Liu, X.; Zhang, X.; Che, R. Vortex tuning magnetization configurations in porous Fe₃O₄ nanotube with wide microwave absorption frequency. *Nano Res.* **2022**, *15*, 6743. [[CrossRef](#)]
50. Salazar-Cardona, M.M.; Korber, L.; Schultheiss, H.; Lenz, K.; Thomas, A.; Nielsch, K.; Kakay, A.; Otálora, J.A. Nonreciprocity of spin waves in magnetic nanotubes with helical equilibrium magnetization. *Appl. Phys. Lett.* **2021**, *118*, 262411. [[CrossRef](#)]
51. Saavedra, E.; Castillo-Sepúlveda, S.; Corona, R.M.; Altbir, D.; Escrig, J.; Carvahlo-Santos, V.L. Influence of curvature on the dynamical susceptibility of bent nanotubes. *Results Phys.* **2022**, *35*, 105290. [[CrossRef](#)]
52. Saavedra, E.; Vidal-Silva, N.; Escrig, J. Dynamic susceptibility of permalloy wire-tube nanostructures. *Results Phys.* **2021**, *31*, 104874. [[CrossRef](#)]
53. Su, X.; Liu, Y.; Liao, Z.; Bi, Y.; Chen, Y.; Ma, Y.; Chung, K.L.; Wan, F.; Ma, M. A review of 1D magnetic nanomaterials in microwave absorption. *J. Mater. Sci.* **2023**, *58*, 636. [[CrossRef](#)]
54. Vansteenkiste, A.; Leliaert, J.; Dvornik, M.; Helsen, M.; García-Sánchez, F.; Van Waeyenberge, B. The design and verification of MuMax3. *AIP Adv.* **2014**, *4*, 107133. [[CrossRef](#)]
55. Gilbert, T.L. A phenomenological theory of damping in ferromagnetic materials. *IEEE Trans. Magn.* **2004**, *40*, 3443. [[CrossRef](#)]
56. Kolhatkar, A.G.; Jamison, A.C.; Litvinov, D.; Willson, R.C.; Lee, T.R. Tuning the magnetic properties of nanoparticles. *Int. J. Mol. Sci.* **2013**, *14*, 15977. [[CrossRef](#)]
57. Xiang, H.; Jiang, D.M.; Yao, J.C.; Zheng, Y.P.; Lu, W.; Li, G.Q.; Saito, H.; Ishio, S.; Tan, X.W.; Lin, Y.Q. Micromagnetic simulations of magnetization reversal of iron nanowire. *J. Phys. Conf. Ser.* **2011**, *266*, 012022. [[CrossRef](#)]
58. Ruiz-Gomez, S.; Pérez, L.; Mascaraque, A.; Quesada, A.; Prieto, P.; Palacio, I.; Martín-García, L.; Foerster, M.; Aballe, L.; de la Figuera, J. Geometrically defined spin structures in ultrathin Fe₃O₄ with bulk like magnetic properties. *Nanoscale* **2018**, *10*, 5566. [[CrossRef](#)]
59. Dao, N.; Donahue, M.J.; Dumitru, I.; Spinu, L.; Whittenburg, S.L.; Lodder, J.C. Dynamic susceptibility of nanopillars. *Nanotechnology* **2004**, *15*, S634. [[CrossRef](#)]
60. Chen, W.B.; Han, M.G.; Zhou, H.; Yu, O.; Deng, L.G. Micromagnetic simulation on the dynamic susceptibility spectra of cobalt nanowires arrays: The effect of magnetostatic interaction. *Chin. Phys. B* **2010**, *19*, 087502.
61. Lupo, P.; Kumar, D.; Adeyeye, A.O. Size dependence of spin-wave modes in Ni₈₀Fe₂₀ nanodisks. *AIP Adv.* **2015**, *5*, 077179. [[CrossRef](#)]
62. Dobrovolskiy, O.V.; Bunyaev, S.A.; Vovk, N.R.; Navas, D.; Gruszecki, P.; Krawczyk, M.; Sachser, R.; Huth, M.; Chumak, A.V.; Guslienko, K.Y.; et al. Spin-wave spectroscopy of individual ferromagnetic nanodisks. *Nanoscale* **2020**, *12*, 21207. [[CrossRef](#)] [[PubMed](#)]
63. Yang, J.; Kim, J.; Kim, B.; Cho, Y.J.; Lee, J.H.; Kim, S.K. Vortex-chirality-dependent standing spin-wave modes in soft magnetic nanotubes. *J. Appl. Phys.* **2018**, *123*, 033901. [[CrossRef](#)]

Disclaimer/Publisher's Note: The statements, opinions and data contained in all publications are solely those of the individual author(s) and contributor(s) and not of MDPI and/or the editor(s). MDPI and/or the editor(s) disclaim responsibility for any injury to people or property resulting from any ideas, methods, instructions or products referred to in the content.